

Article

Layered Organic Conductors Based on BEDT-TTF and Ho, Dy, Tb Chlorides

Alexandra M. Flakina ^{*}, Elena I. Zhilyaeva ^{*} , Gennady V. Shilov, Maxim A. Faraonov, Svetlana A. Torunova and Dmitri V. Konarev ^{*}

Federal Research Center of Problems of Chemical Physics and Medicinal Chemistry,
Russian Academy of Sciences, 142432 Chernogolovka, Russia

^{*} Correspondence: flakina@icp.ac.ru (A.M.F.); zhilya@icp.ac.ru (E.I.Z.); konarev3@yandex.ru (D.V.K.)

Abstract: Molecular semiconductors with lanthanide ions have been synthesized based on BEDT-TTF and lanthanide chlorides: (BEDT-TTF)₂[HoCl₂(H₂O)₆]Cl₂(H₂O)₂ (**1**, which contains a 4*f* holmium cation), and (BEDT-TTF)₂LnCl₄(H₂O)_{*n*} (Ln = Dy, Tb, Ho (**2–4**), which contain 4*f* anions of lanthanides). Conductivity and EPR measurements have been carried out along with the SQUID magnetometry, and the crystal structure has been established for **1**. The structure of **1** is characterized by an alternation of organic radical cation layers composed of BEDT-TTF chains and inorganic layers consisting of chains of the [HoCl₂(H₂O)₆]⁺ cations interlinked by chlorine anions and crystallization water molecules. The magnetic susceptibility of **1–3** determined mainly by lanthanide ions follows the Curie–Weiss law with the Weiss temperatures of –3, –3, –2 K for **1–3**, respectively, indicating weak antiferromagnetic coupling between paramagnetic lanthanide ions. The signals attributed to the BEDT-TTF^{•+} radical cations only are observed in the EPR spectra of **1–3**, which makes it possible to study their magnetic behavior. There are two types of chains in the organic layers of **1**: the chains composed of neutral molecules and those formed by BEDT-TTF^{•+} radical cations. As a result, uniform 1D antiferromagnetic coupling of spins is observed in the BEDT-TTF^{•+} chains with estimated exchange interaction $J = -10$ K. The study of dynamic magnetic properties of **1–3** shows that these compounds are not SMMs.

Keywords: radical cation salts; lanthanides; 4*f*-cation; crystal structure; electrical conductivity



Citation: Flakina, A.M.; Zhilyaeva, E.I.; Shilov, G.V.; Faraonov, M.A.; Torunova, S.A.; Konarev, D.V. Layered Organic Conductors Based on BEDT-TTF and Ho, Dy, Tb Chlorides.

Magnetochemistry **2022**, *8*, 142.

<https://doi.org/10.3390/magnetochemistry8110142>

<https://doi.org/10.3390/magnetochemistry8110142>

Academic Editor: Marius Andruh

Received: 11 October 2022

Accepted: 25 October 2022

Published: 28 October 2022

Publisher's Note: MDPI stays neutral with regard to jurisdictional claims in published maps and institutional affiliations.



Copyright: © 2022 by the authors. Licensee MDPI, Basel, Switzerland. This article is an open access article distributed under the terms and conditions of the Creative Commons Attribution (CC BY) license (<https://creativecommons.org/licenses/by/4.0/>).

1. Introduction

Organic radical cation salts of the tetrathiafulvalene family containing unpaired electrons in conducting layers have attracted the attention of researchers with the possibility of influencing the properties of these layers by designing inorganic anions. Depending on their anion nature, compounds of this group exhibit some phenomena and properties interesting for solid state physics [1], such as superconductivity [2], state of quantum spin [3] and quantum dipole [4] liquids, and incoherent interlayer electron transport [5]. To date, among the compounds of this family, molecular conductors based on bis(ethylenedithio)tetrathiafulvalene (BEDT-TTF) and analogues—bis(ethylenedioxy)tetrathiafulvalene (BEDO-TTF) and bis(ethylenedithio)tetraselenafulvalene (BETS) have most widely been studied [1,2,6–8].

The layered packing mode, which is characteristic of compounds based on them, makes it possible to combine in one structure layers of organic radical cations, which determine the conductivity, and anionic layers, which show other properties, thus forming multifunctional hybrid systems. Single-molecule magnets (SMMs) emerged in 1993 when the coordination compound Mn12-ac was investigated [9]. Lately, many different SMMs have been studied. Generally, they show frequency-dependent peaks in the χ_M'' plots, the hysteresis cycle is open for the field dependence of the magnetization, and the FC (Field Cooled) and ZFC (Zero-Field Cooled) magnetic susceptibility curves are different at some

temperatures [9,10]. The recent use of SMMs as anions in combination with BEDO-TTF has led to the occurrence of hybrid multifunctional materials, which exhibit high conductivity and single-molecule magnetism at low temperatures and have the composition β'' -(BEDO-TTF)₄[Co(pdms)₂·3H₂O] [11] and β'' -(BEDO-TTF)₄[ReF₆]·6H₂O [12]. These properties are manifested at low temperatures. Nevertheless, it is expected that the combination of conductive layers of tetrathiafulvalenes and anionic layers with magnetic properties in the same compound can lead to the emergence of new properties in such hybrid materials. Therefore, the search for organic conductors with lanthanide ions containing 4*f*-electrons is underway. The 4*f*-elements are characterized by the co-existence of its *f*-orbital spins and high magnetic moments, and they could exhibit interesting magnetic properties in a joint structure with organic BEDT-TTF radical cations. Several BEDT-TTF salts with lanthanide anions characterized by now are semiconductors [13–15]. BEDT-TTF salts with lanthanide chlorides (Yb, Sm, Nd, and Ce) are shown to be air-sensitive, and their crystal structures and magnetic properties are not determined [16].

In this work, hybrid compounds based on BEDT-TTF and lanthanide chlorides have been obtained. (BEDT-TTF)₂[HoCl₂(H₂O)₆]Cl₂(H₂O)₂ (**1**) contains cations of two types, namely, organic BEDT-TTF⁺ radical cations and inorganic [HoCl₂(H₂O)₆]⁺ cations, and Cl[−] anions. (BEDT-TTF)₂LnCl₄(H₂O)_{*n*}, Ln = Dy, Tb, Ho (hereinafter **2**, **3**, **4**) contain lanthanide 4*f*-anions. The conductivity of **1–4** has been measured, an EPR and SQUID measurements of **1–3** have been carried out, and the crystal structure of **1** has been established and discussed.

2. Results and Discussion

2.1. Synthesis

Crystals of double salt **1** containing BEDT-TTF⁺ cations and a complex inorganic holmium (III) cation were obtained by electrocrystallization in the presence of electrolyte of [NBu₄]₃HoCl₆·*m*H₂O stoichiometry in 1,2-dichlorobenzene containing 2% ethanol. To synthesize **2–4**, we used chloro- or 1,2-dichloro-benzene as a solvent without adding ethanol. A significant problem in the study of these crystals is the selection of a crystal suitable for X-ray analysis since they are the thinnest plates. The compounds are hygroscopic and gradually degrade during long-term storage in air.

2.2. Conductivity

The room-temperature conductivities of **1**, **2**, **3**, and **4** single crystals are 0.004, 0.007, 0.0008, and 0.035 S/cm. The dependence of the logarithm of relative resistivity on reciprocal temperature for these compounds (Figure 1) shows that they are semiconductors with an activation energy of conductivity of 0.22 eV, 0.30 eV, 0.32, and 0.29 eV, respectively.

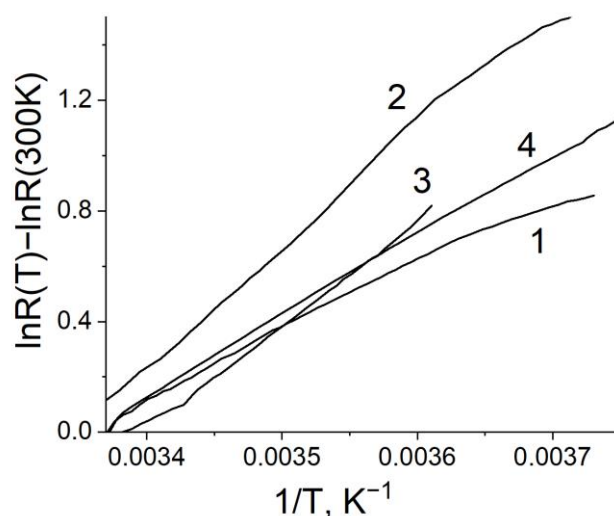


Figure 1. Dependence of logarithm of relative resistivity of **1–4** on reciprocal temperature.

2.3. Crystal Structure of (BEDT-TTF)₂[HoCl₂(H₂O)₆]Cl₂(H₂O)₂

The crystal structure of **1** has been determined from X-ray structural analysis at 100 K. The salt crystallizes in the monoclinic system. The structure has been determined and refined in space group *C2/c*. The asymmetric part includes two halves of the BEDT-TTF molecule located near the inversion centers, half of the [HoCl₂(H₂O)₆]⁺ cation at the inversion center, the Cl[−] anion, and a crystallization water molecule. The unit cell parameters are given in Table 1. The composition of (BEDT-TTF)₂[HoCl₂(H₂O)₆]Cl₂(H₂O)₂ has been determined from an X-ray study.

Table 1. Crystal data and structure refinement for **1**.

Empirical Formula	C ₂₀ H ₃₂ Cl ₄ HoO ₈ S ₁₆
Formula weight	1220.14
Temperature, K	100.01 (10) K
Wavelength, Å	0.7107
Crystal system, space group	Monoclinic, <i>C2/c</i>
<i>a</i> , Å	15.6323 (7)
<i>b</i> , Å	6.3164 (2)
<i>c</i> , Å	40.9243 (18)
α , deg.	90
β , deg.	91.057 (4)
γ , deg.	90
Cell volume, Å ³	4040.2 (3)
<i>Z</i> ; <i>d</i> _{calc} , g cm ^{−3}	4, 2.006
Absorption coefficient, mm ^{−1}	3.092
<i>F</i> (000)	2428
Crystal size, mm	0.20 × 0.10 × 0.06
Theta range, deg.	2.987 to 29.068
Limiting indices	−14 ≤ <i>h</i> ≤ 21, −8 ≤ <i>k</i> ≤ 7, −55 ≤ <i>l</i> ≤ 49
Reflections collected/unique	9605/5416 [R (int) = 0.0430]
Completeness to theta = 25.242	99.8%
Data/restraints/parameters	5416/166/319
Absorption correction	Semi-empirical from equivalents
Max. and min. transmission	1.00000 and 0.96636
Refinement method	Full-matrix least-squares on <i>F</i> ²
Goodness-of-fit on <i>F</i> ²	1.243
Final <i>R</i> indices [<i>I</i> > 2σ(<i>I</i>)]	<i>R</i> 1 = 0.0803, <i>wR</i> 2 = 0.1511
<i>R</i> indices (all data)	<i>R</i> 1 = 0.0925, <i>wR</i> 2 = 0.1567
Largest diff. peak and hole	2.944 and −3.051 e Å ^{−3}

In the crystal structure of **1**, the organic radical cation layers of BEDT-TTF alternate with layers of [HoCl₂(H₂O)₆]⁺ cations and molecules of crystallization water along the *c* axis; these cationic layers are interlinked by chlorine anions Cl[−] (Figure 2).

The salt has two crystallographically unique donor-molecule layers in the unit cell. In one BEDT-TTF layer (Layer I), radical cations are packed into stacks along the *a*+*b* direction, and in the other one (Layer II), they are packed along the *a*-*b* direction. The angle between these directions is ~44°. The structure of these layers is the same.

Two independent BEDT-TTF molecules designated in Figure 3 as C1 and C6 alternate in each stack, the central C=C double bonds of neighboring molecules being at the same distance from each other (~4.21 Å). Each independent BEDT-TTF molecule is disordered over two positions. This disorder can be represented as a slight rotation of the plane drawn through sulfur atoms about the central C=C bond (Figure 3a). The dihedral angle between the planes of these two positions is approximately ~43°.

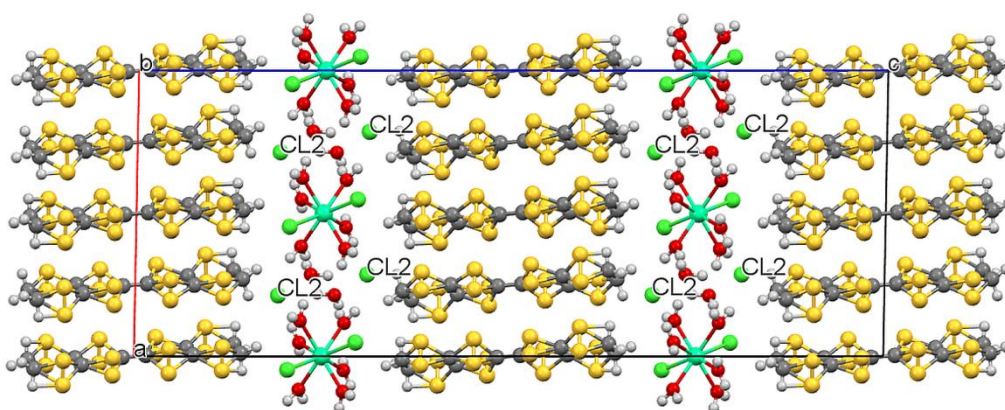


Figure 2. General view of the crystal structure of **1**. Organic and inorganic cation layers are interlinked by chloride anions Cl2.

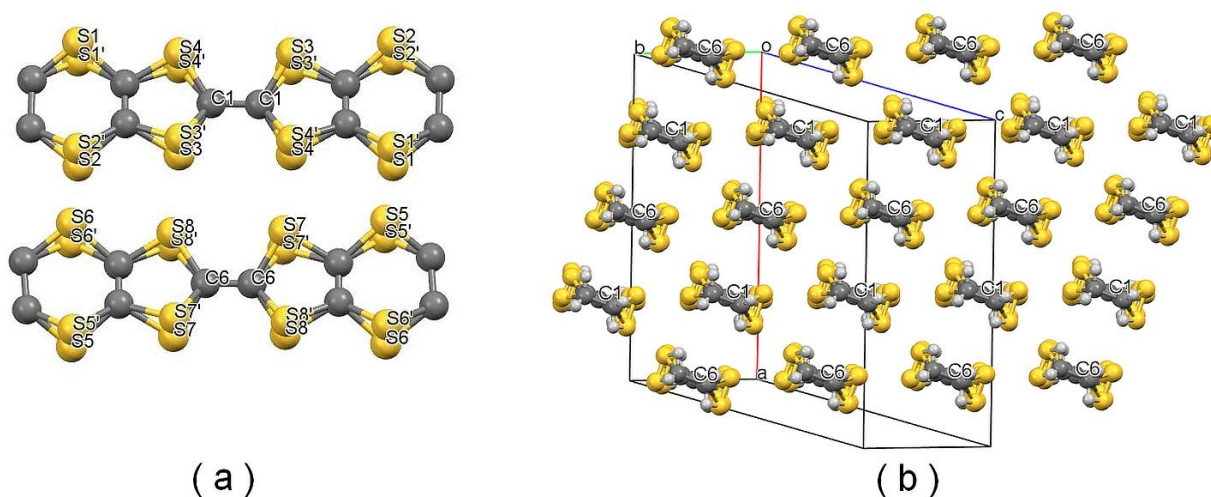


Figure 3. (a) The molecular structure of the radical cation part of **1**. The radical cations are disordered in two positions. In one of the positions, sulfur atoms are designated as S. In another position, they are designated as S'. (b) View of radical cation layer I along the direction of the central C=C double bond of the BEDT-TTF molecule.

The lengths of the central C=C bonds for independent molecules are different: 1.386(17) Å for the C1=C1 bond and 1.339(18) Å for the C6=C6 bond. These values are close to the bond lengths of 1.375(28) Å [17] for the BEDT-TTF⁺ radical cation and 1.343(4) Å [18] for the uncharged BEDT-TTF⁰ molecule, which allows us to conclude that charge disproportionation is observed in the organic layer which provides the formation of BEDT-TTF⁺ and BEDT-TTF⁰.

Several options for the structure of the organic layer can be proposed based on the presence of two orientations for the BEDT-TTF molecules. Such a layer can be considered as a superposition of two layers with stacks of parallel molecules (Figure 4a) or as a superposition of two layers of another type when the molecules in the stack are not parallel but arranged in a zigzag pattern (Figure 4b).

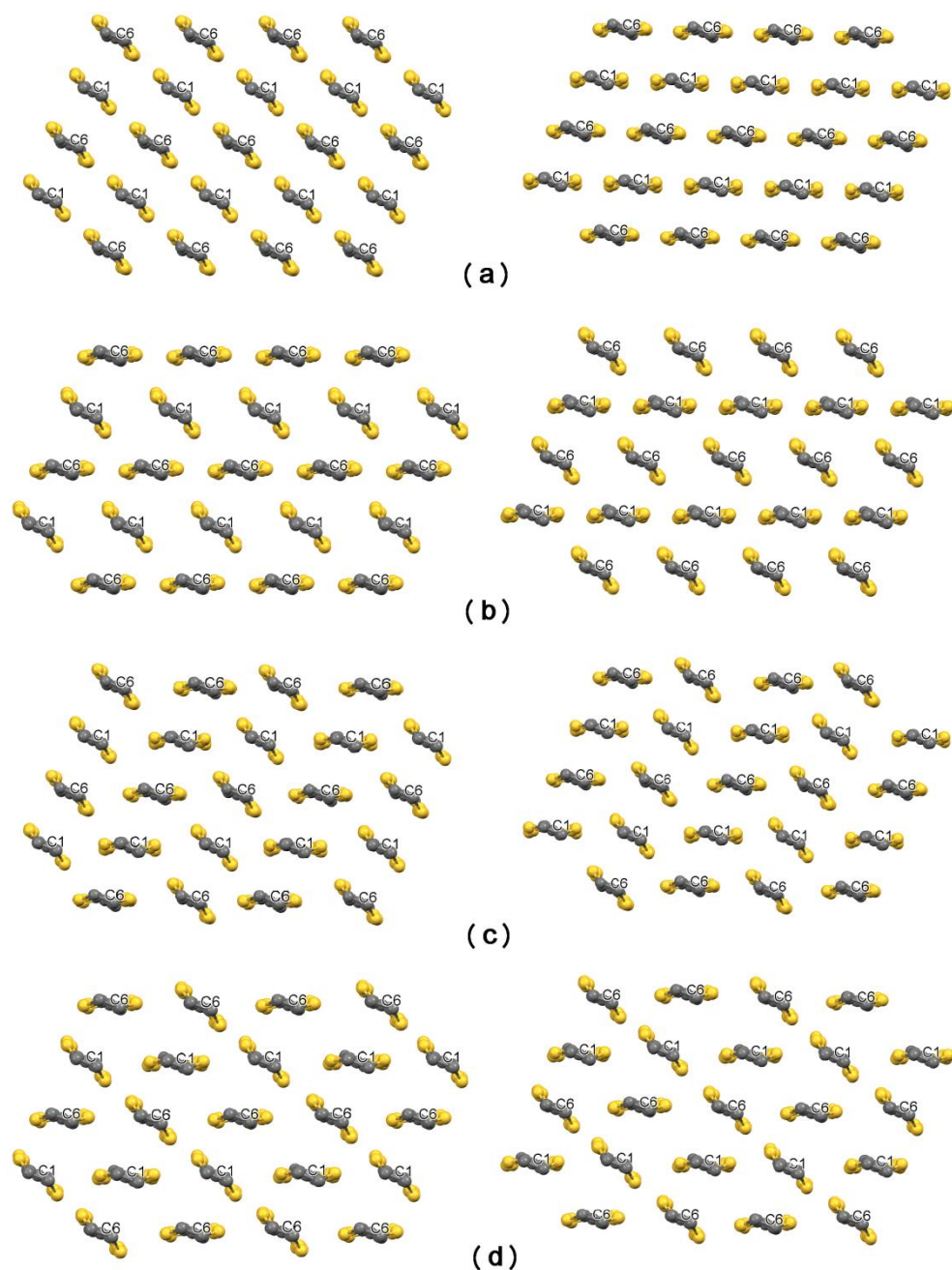


Figure 4. Options for the structure of the organic radical cation layer in **1**. For each of cases (a–d) the left and right panels show two variants of the structure of the BEDT-TTF layer, the superposition of which could lead to the structure shown in Figure 3b.

In case (a), the BEDT-TTF molecules form ribbons in the transverse direction. The S . . . S contacts are observed only in ribbons, and the distances between the molecules in the stacks are quite long. In case (b), the molecules in the stack are arranged in a zigzag pattern, and the radical cations inside the stacks are linked by shortened S . . . S contacts. In both cases (a) and (b), either uncharged BEDT-TTF molecules or BEDT-TTF^{•+} radical cations located in the ribbons have abnormally short side-by-side contacts S . . . S (~3.06–3.07 Å), which are never observed in the BEDT-TTF salts. Therefore, options (a) and (b) cannot be realized in a crystal.

Since the radical cation part of the structure is disordered, we tried to combine the options in such a way that abnormally short side-by-side S . . . S contacts could be avoided. This combination resulted in two possible options, Figure 4c,d. For these options, there

are S...S contacts of 3.37–3.69 Å length (Figure S1, Supplementary Materials) characteristic of BEDT-TTF salts. In both cases, there are two types of chains with non-parallel BEDT-TTF-units: the chains composed of uncharged molecules (molecules C6 in Figure 4) and similar chains composed of BEDT-TTF⁺ radical cations (molecules C1 in Figure 4). When averaged, each option gives two disordered BEDT-TTF molecules found when solving the structure.

The crystal structure of **1** contains inorganic cation layers of [HoCl₂(H₂O)₆]⁺ cations along with organic cation layers. The organic and inorganic cation layers are separated by Cl₂ anions (Figure 2). In the inorganic cation layer, the holmium (III) atom is surrounded by eight ligands: two chloride anions Cl1 and six water molecules, which give a distorted square antiprism surrounding the holmium atoms (Figure 5a).

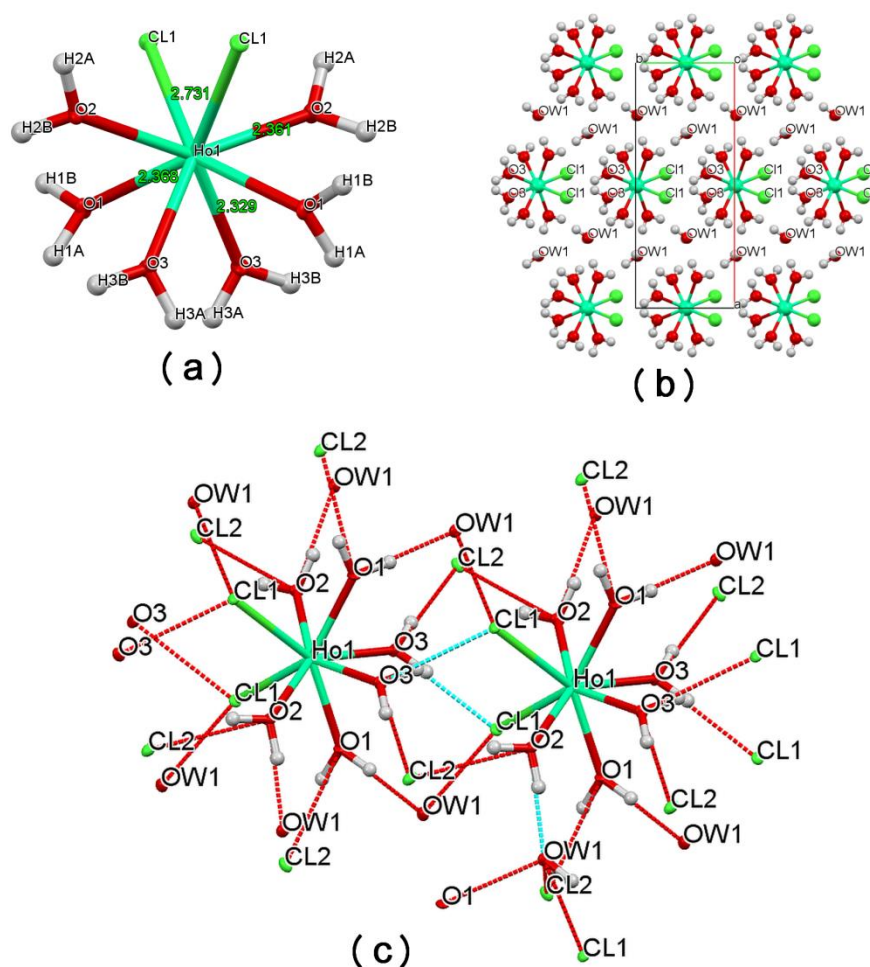


Figure 5. (a) Structure of the [HoCl₂(H₂O)₆]⁺ cation in **1**. (b) Chains of holmium cations. (c) A fragment of the inorganic layer showing hydrogen bonds of the Ho (III) ligand environment with crystallization water molecules OW1 and chlorine anions Cl₂ located between the organic and inorganic cation layers.

The [HoCl₂(H₂O)₆]⁺ cations form infinite chains along the *b* direction due to the hydrogen bonds between two water molecules of one polyhedron (denoted as O3 in Figure 5b) and two Cl1 chlorine atoms of the neighboring polyhedron. The Ho...Ho distance in the chain is 6.316 Å. The crystallization water molecules (denoted as OW1) are located in the layer parallel to the chains. The ligands of the [HoCl₂(H₂O)₆]⁺ cations belonging to the adjacent chains form the shortened O–H...O and Cl1...H–O contacts with crystallization water molecules OW1 in the transverse direction and shortened O–H...Cl2 contacts with chlorine anions Cl₂ located between the organic and inorganic cation layers (Figure 5c), forming a continuous network of hydrogen bonds parallel to the *ab* plane

of the unit cell. The nearest distance between two Ho (III) atoms from neighboring chains is 8.43 Å. Table 2 shows the parameters of the hydrogen bonds in the inorganic layers of **1**.

Table 2. Hydrogen bonds in the inorganic layers.

D-H	d(D-H, Å)	d(H..A, Å)	<DHA, deg.	d(D..A, Å)	A
O1-H1A	0.953	1.792	174.35	2.742	OW1 [x + 1/2, y + 1/2, z]
O1-H1B	0.951	2.243	154.94	3.130	Cl2 [x - 1/2, y - 1/2, z]
O2-H2A	0.949	2.327	160.56	3.238	Cl2 [x - 1, y - 1, z]
O2-H2B	0.954	1.735	172.10	2.683	OW1
O3-H3A	0.948	2.183	161.18	3.095	Cl1 [x, y + 1, z]
O3-H3B	0.951	2.102	172.17	3.047	Cl2 [x - 1, y, z]
OW1-HW1A	0.947	2.161	164.99	3.085	Cl2 [-x - 1/2, y - 1/2, -z + 1/2]
OW1-HW1B	0.946	2.335	142.87	3.141	Cl1 [x - 1/2, y + 1/2, z]

The composition of **2**, **3**, and **4**, determined with an electron probe microanalysis, is (BEDT-TTF)₂LnCl₄(H₂O)_n. Unfortunately, we were unable to determine the crystal structure of these compounds due to the low quality of the crystals. The X-ray powder diffractograms of **2** and **3** are similar (Figures S2 and S3, Supplementary Materials), showing that these compounds are isostructural to each other. They are different from the simulated X-ray powder diffractogram of **1** (Figure S4, Supplementary Materials), and, hence, **2** and **3** are not isostructural to **1**.

A preliminary X-ray study of **4** prepared similarly to **2** and **3** in ethanol-free solvent reveals the [HoCl₄(H₂O)₄]⁻ anion (Figure S5, Supplementary Materials). We failed to resolve the structure of the BEDT-TTF radical cation layers in **4**.

2.4. SQUID Magnetometry

The magnetic susceptibility of **1**, **2**, and **3** were measured from 300 to 1.9 K and back in anaerobic conditions on a SQUID magnetometer. The temperature dependences of molar magnetic susceptibility of the studied compounds are shown in Figures S6a–c, Supplementary Materials. Figure 6 shows the effective magnetic moment of **1–3** as a function of temperature.

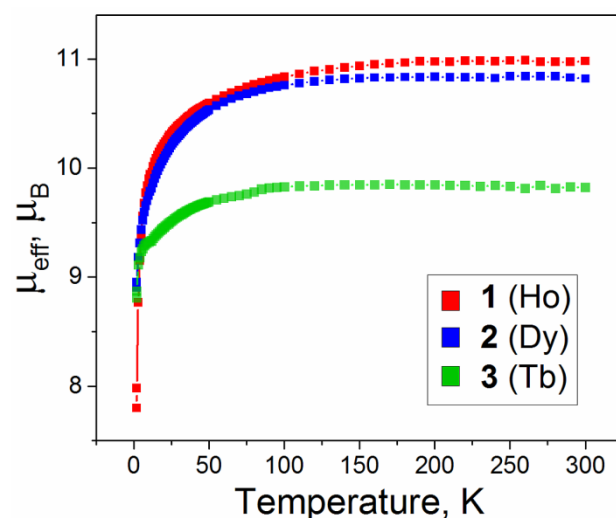


Figure 6. Temperature dependence of effective magnetic moment of **1**, **2**, and **3**.

The effective magnetic moment is 10.98 μ_B for **1** with holmium (χ_MT value is 15.07 emu·K/mol per formula unit), 10.81 μ_B for **2** with dysprosium (χ_MT value is 14.65 emu·K/mol per formula unit), and 9.82 μ_B for **3** with terbium (χ_MT value is 12.05 emu·K/mol per formula unit), respectively (Figure 6). These values are somewhat higher than expected for isolated Ho (III), Dy (III), and Tb (III) ions, which have electronic

configuration 5I_8 ; $^6H_{15/2}$; 7F_6 at g-factors of 5/4, 4/3, and 3/2 and the expected value of the magnetic moment equal to 10.31, 10.65, and 9.72 μ_B , respectively [19].

Apparently, the paramagnetic BEDT-TTF⁺ radical cations, which have spin state $S = 1/2$, make an additional contribution to the magnetic susceptibility of each salt. However, the magnitude value of this contribution shows that it is insignificant as compared to the contribution from the paramagnetic ions of Ho(III), Dy(III), and Tb(III).

Similarly, it was shown previously that, for example, effective magnetic moment $\mu_{\text{eff}} = 9.88 \mu_B$ for {Cryptand [2.2.2] (Na⁺)₂}{(Pc²⁻) Tb^{III} (Pc³⁻)₂}⁻ with Tb(III) and additional spin $S = 1/2$ on phthalocyanine (Pc³⁻) [20] only slightly exceeds the value expected for the Tb(III) magnetic moment of 9.72 μ_B .

The temperature dependencies of the reciprocal molar magnetic susceptibility are shown in Figures S6d, S6e, and S6f, Supplementary Materials. In the entire temperature range (1.9–300 K), reciprocal molar susceptibility is described by the Curie–Weiss law with Weiss temperatures of –3, –3, and –2 K, respectively, indicating weak antiferromagnetic interactions between the paramagnetic Ho (III), Dy (III), and Tb (III) ions. This may be due to the fact that the magnetic interactions between ions can be transmitted through a system of hydrogen bonds between diamagnetic water molecules and chloride ions. Generally, it is not a very efficient way to transfer magnetic interactions between paramagnetic centers [21].

The dynamic magnetic properties of **1**, **2**, and **3** have been studied by SQUID at 3.0-Oe *ac* field at frequencies of 1–1500 Hz. The compounds do not exhibit the properties of single-molecule magnets (SMMs). That means they do not show any peaks in the χ_M'' plots, the hysteresis cycle for the field dependence of the magnetization is not observed, and there is no difference between FC and ZFC magnetic susceptibility curves down to 2K.

Despite the fact that the contribution from BEDT-TTF⁺ radical cations is almost indistinguishable against the background of high magnetic moments of paramagnetic lanthanides, the magnetic behavior of the organic layer can be analyzed using the data of EPR measurements since these radical cations show intense EPR signals, and paramagnetic lanthanide ions are not manifested in the EPR spectra in the entire studied temperature range (4.2–293 K). The reason may be high zero-field splitting, which takes place for dysprosium, terbium, and holmium ions and which usually significantly exceeds the energy of a microwave quantum at X-band EPR [22,23].

2.5. EPR Measurements

The EPR spectra of **1–3** are single intense Lorentz lines with g-factor at room temperature $g \sim 2.0060$ characteristic of BEDT-TTF⁺ radical cations (Figures 7 and S7 and S8). The linewidth (ΔH_{pp}) at room temperature is ~ 4.6 mT for **1** and ~ 2.8 mT for **2** and **3**. The difference in ΔH_{pp} suggests the different structures of the radical cation layers in **1** and **2–3** and is consistent with the X-ray powder diffractograms data. The lines narrow noticeably with decreasing temperature. Below 100, 170, and 30 K (for **1**, **2**, and **3**, respectively), there is a noticeable distortion in the shape of the BEDT-TTF⁺ signal lines from the Lorentz shape, and the signal is better described by two Lorentz lines for **1** and **3**, and three Lorentz lines for **2**. In this case, the lines shift towards higher and lower values at low temperatures and slightly broaden (Figures 7 and S7–S10), which can be attributed to the implementation of antiferromagnetic interactions in the BEDT-TTF layers.

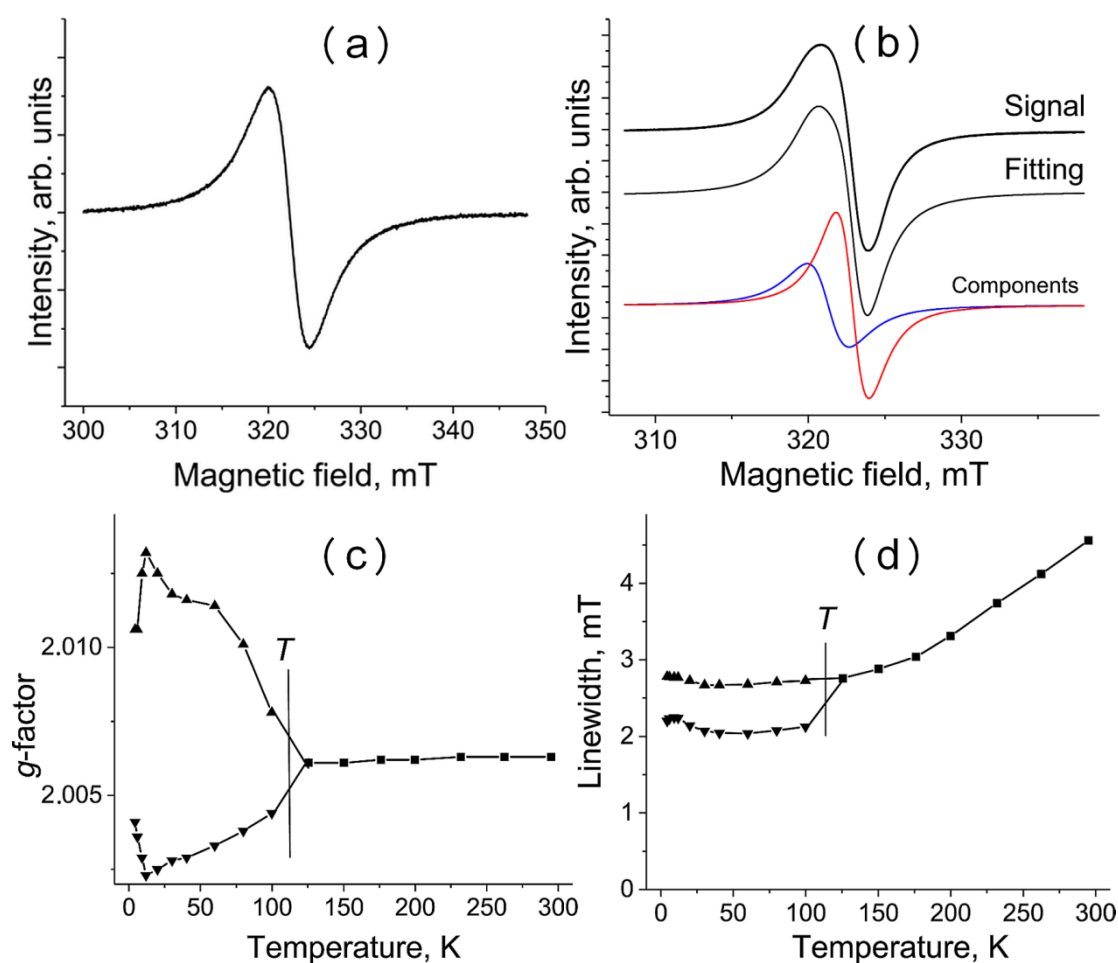


Figure 7. (a,b) EPR signal from **1** at 295 K and 20 K. An approximation of the signal by two Lorentz lines at 12 K is shown at the bottom of the figure. (c,d) Temperature dependencies of EPR signal parameters for **1**: (c) g -factor and (d) linewidth. “ T ” denotes the temperature of splitting of the EPR signal into two Lorentz lines.

Figure 8 shows the temperature dependence of the integral intensity of the two components of the EPR signal from BEDT-TTF⁺ for **1**. The maximal integral intensity of the EPR signal is observed at 12 K, after which the signal intensity decreases due to the antiferromagnetic ordering of spins in the BEDT-TTF⁺ chains. This magnetic behavior is described well enough by the Heisenberg model for a one-dimensional (1D) chain of antiferromagnetically interacting spins with an exchange energy J equal to -10 K (Figure 8), which is consistent with the position of the maximum on the curve at about 12 K. Thus, the antiferromagnetic ordering of spins in the 1D chains is observed in the BEDT-TTF⁺ chains. The absence of strong antiferromagnetic exchange between BEDT-TTF⁺ is stipulated by the absence of strong π - π interactions between them (there are only short side-by-side S...S contacts between them) (Figure S1, Supplementary Materials). Seemingly, there is no magnetic exchange between the chains in the BEDT-TTF layer since the radical cation chains are separated by chains of uncharged diamagnetic BEDT-TTF molecules (Figure 4c,d).

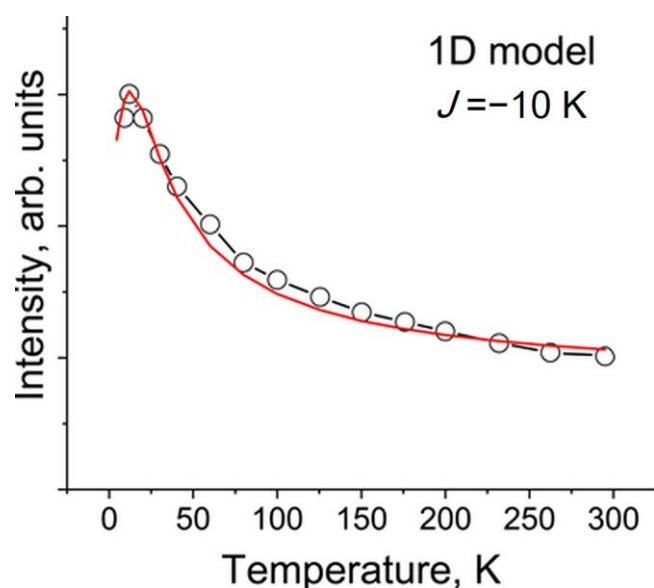


Figure 8. Temperature dependence of integral intensity of the two components of the EPR signal from BEDT-TTF⁺ (open circles) of salt **1** and fitting of these data by the Heisenberg model for 1D chains of uniformly antiferromagnetically interacting spins (red curve) [24,25].

The temperature dependencies of the *g*-factor and linewidth of EPR signals for **2** and **3** are presented in Figures S9 and S10.

Thus, new semiconductors based on BEDT-TTF containing 4*f*-complexes of cationic and anionic lanthanide chlorides have been synthesized. The crystal structure of (BEDT-TTF)₂[HoCl₂(H₂O)₆]Cl₂(H₂O)₂ is characterized by alternating organic radical cation layers built from 1D BEDT-TTF⁺ chains and BEDT-TTF⁰ chains and inorganic layers from cation chains [HoCl₂(H₂O)₆]⁺ bound together by chlorine anions and crystallization water molecules. The compounds do not exhibit the properties of SMMs.

3. Materials and Methods

3.1. Reagents

BEDT-TTF (98%, Sigma-Aldrich, Steinheim, Germany), *o*-dichlorobenzene (99%, Sigma-Aldrich, Steinheim; Germany), chlorobenzene (99%, ACROS Organics, Geel, Belgium), Bu₄NCl (97%, Fluka, Buchs, Switzerland), LnCl₃·6H₂O, Ln = Ho, Dy, Tb (chemically pure, AntrazoXrom, Moscow, Russia) were used without preliminary purification.

3.2. Synthesis

3.2.1. Synthesis of Electrolytes of Stoichiometry (NBu₄)₃LnCl₆·mH₂O

Electrolytes were obtained by adding LnCl₃·6H₂O (1 mmol) to 6 mL of a solution of NBu₄Cl (0.8325 g, 3 mmol) in acetone, stirring for ~2 h at 30 °C, and filtering the solution into diethyl ether (30–40 mL). The resulting oily product was turned into a powder by stirring on a magnetic stirrer for 1–2 h, filtered, washed with ether, and dried in a desiccator over CaCl₂ for two days. Yield 60–80%.

3.2.2. Synthesis of (BEDT-TTF)₂[HoCl₂(H₂O)₆]Cl₂(H₂O)₂ (**1**)

A solution of 5.8 mg (0.015 mmol) of BEDT-TTF in 4 mL of *o*-dichlorobenzene was placed in the anode compartment of the electrochemical cell. A solution of 45 mg (0.03 mmol) of the [NBu₄]₃HoCl₆·7H₂O electrolyte in a mixture of *o*-dichlorobenzene/ethanol (8 mL/0.2 mL) was poured into the compartments of the cell to the same level. Electrochemical oxidation was carried out in the galvanostatic mode (*I* = 0.8 μA) at *T* = 25 °C. Crystals in the form of dark brown plates were obtained within 2 weeks. The composition of **1** was determined from single crystal X-ray diffraction analysis (Agilent XCalibur CCD diffractometer, Agilent

Technologies UK Ltd., Yarnton, Oxfordshire, UK) in combination with electron probe microanalysis (EPMA) (LEO SUPRA 25, Carl Zeiss, Oberkochen, Germany).

3.2.3. Synthesis of $(\text{BEDT-TTF})_2[\text{HoCl}_4(\text{H}_2\text{O})_4](\text{H}_2\text{O})_x$ (4)

A solution of 5.2 mg (0.0135 mmol) of BEDT-TTF in 4 mL of chlorobenzene was placed in the anode compartment of an electrochemical cell, an electrolyte solution of $(\text{NBu}_4)_3\text{HoCl}_6 \cdot 7\text{H}_2\text{O}$ (24.6 mg, 0.02 mmol) in 5 mL of chlorobenzene was distributed between the cathode and anode compartments to the same level. Electrochemical oxidation was carried out in galvanostatic mode ($I = 0.3 \mu\text{A}$) at $T = 18^\circ\text{C}$. The crystals were obtained within 3 weeks. The composition was determined from electron probe microanalysis (EPMA), and the structure of the anion was determined by preliminary X-ray diffraction analysis.

3.2.4. Synthesis of $(\text{BEDT-TTF})_2\text{LnCl}_4(\text{H}_2\text{O})_n$, Ln = Dy, Tb (2, 3)

A solution of 5.8 mg (0.015 mmol) of BEDT-TTF in 4 mL of *o*-dichlorobenzene (2) or 5 mL of chlorobenzene (3) was placed in the anode compartment of the electrochemical cell. A solution of 0.03 mmol of electrolyte in 5–8 mL of the corresponding solvent was poured into the compartments of the cell to the same level. Electrochemical oxidation was carried out in galvanostatic mode ($I = 0.1\text{--}0.4 \mu\text{A}$) at $18\text{--}25^\circ\text{C}$. Crystals in the form of the thinnest brown plates were obtained within 2–3 weeks. The composition was determined from EPMA.

3.3. Single Crystal X-ray Analysis

The X-ray diffraction experiment was carried out on an Agilent XCalibur CCD diffractometer with an EOS detector (Agilent Technologies UK Ltd., Yarnton, UK). Data collection, processing, determination, and the refinement of the unit cell parameters were performed using the CrysAlis PRO package [26].

The crystals were studied at 100 K. The structure was solved by a direct method. The positions and thermal parameters of non-hydrogen atoms were refined in the isotropic and then in the anisotropic approximation by the full-matrix least-squares method (LSM).

The positions of the hydrogen atoms of the water molecules were revealed from difference syntheses and refined with restrictions on bond lengths. The BEDT-TTF molecules are disordered, the positions of carbon atoms were revealed from the difference syntheses, and the positions near them were taken as sulphur atoms.

Taking into account the weak peaks, it turns out that the molecules form a stack of overlapping BEDT-TTFs. Only high electron density peaks were taken from synthesis to refinement, from which two disordered BEDT-TTF molecules were formed. Molecules were refined with a restriction on thermal parameters.

The positions of the hydrogen atoms of the ethylene groups of BEDT-TTF were calculated and refined in the rider scheme. All of the calculations were performed using the SHELX-97 software package [27]. The unit cell parameters and the main crystallographic data are listed in Table 1. Experimental details, atomic coordinates, bond lengths, and bond angles were deposited with the Cambridge Crystallographic Data Center with reference code CCDC 2210175.

3.4. Electric Conductivity

The conductivity of the single crystals of the radical cation salts was measured by a standard four-probe method at a direct current of $10 \mu\text{A}$ with a decrease in temperature from 293 K to 80 K. Gold contacts $10 \mu\text{m}$ in diameter were glued to the crystal using graphite paste.

3.5. EPR Spectroscopy and SQUID Magnetometry

The EPR spectra were recorded for polycrystalline samples of 1–3 with a JEOL JES-TE 200 X-band spectrometer (JEOL Ltd., Tokyo, Japan) equipped with a JEOL ES-CT470

cryostat (JEOL Ltd., Tokyo, Japan) in the temperature range from 295 down to 4 K. A Quantum Design MPMS-XL SQUID magnetometer (Quantum Design Inc., San Diego, CA, USA) was used to measure the static magnetic susceptibility of **1–3** at 100 mT magnetic field in cooling and heating conditions in the 300–1.9 K range. A sample holder contribution and core temperature-independent diamagnetic susceptibility (χ_d) were subtracted from the experimental values. The χ_d values were estimated by the extrapolation of the data in the high-temperature range by fitting the data with the expression: $\chi_M = C/(T - \Theta) + \chi_d$, where C is Curie constant and Θ is Weiss temperature. Effective magnetic moment (μ_{eff}) was calculated with the following formula: $\mu_{\text{eff}} = (8\chi_M T)^{1/2}$.

Supplementary Materials: The following are available online at <https://www.mdpi.com/article/10.3390/magnetochemistry8110142/s1>, Figure S1: Formation of Van der Waals contacts in cation (BEDT-TTF⁺) and neutral (BEDT-TTF⁰) chains and between them for option (c) of the organic layer of **1**; Figure S2: X-ray powder diffractogram for **2**; Figure S3: X-ray powder diffractogram for **3**; Figure S4: Simulated X-ray powder diffractogram for **1**; Figure S5: Structure of [HoCl₄(H₂O)₄][−] anion in **4**; Figure S6: Temperature dependence of molar magnetic susceptibility (S6a, S6b, and S6c) and reciprocal molar magnetic susceptibility (S6d, S6e, S6f) for **1**, **2**, and **3**; Figure S7: EPR signal from **2** at 293, 70, and 4.3 K. The approximation of the signal by one and three orange lines is shown at the bottom of the figures; Figure S8: EPR signal from **3** (with terbium) at 12 and 295 K. The approximation of the signal at 12 K by two Lorentz lines is shown at the bottom of the figure. Figure S9: Temperature dependencies for parameters of EPR signal from **2** (with dysprosium): (a) g -factor and (b) the linewidth. “T” marks the temperature for splitting of EPR signal into three Lorentzian lines; Figure S10: Temperature dependencies for parameters of EPR signal from **3**: (a) g -factor and (b) the linewidth.

Author Contributions: Conceptualization, D.V.K.; Data curation, E.I.Z.; Formal analysis, G.V.S. and D.V.K.; Investigation, A.M.F., E.I.Z., G.V.S., M.A.F., S.A.T. and D.V.K.; Methodology, E.I.Z. All authors have read and agreed to the published version of the manuscript.

Funding: The work was supported by the Ministry of Science and Higher Education of the Russian Federation (Grant No. 075-15-2020-779).

Institutional Review Board Statement: Not applicable.

Informed Consent Statement: Not applicable.

Data Availability Statement: The crystallographic data have been deposited with the Cambridge Crystallographic Data Centre, deposition number CCDC 2210175.

Acknowledgments: EPMA of the samples was carried out using the equipment of the Federal Research Center of Problems of Chemical Physics and Medicinal Chemistry RAS <http://www.icp.ac.ru/en> (accessed on 10 October 2022).

Conflicts of Interest: The authors declare no conflict of interest. The funders had no role in the design of the study; in the collection, analyses, or interpretation of data; in the writing of the manuscript, or in the decision to publish the results.

References

1. Naito, T. Modern History of Organic Conductors: An Overview. *Crystals* **2021**, *11*, 838. [[CrossRef](#)]
2. Williams, J.M.; Ferraro, J.R.; Thorn, R.J.; Carlson, K.D.; Geiser, U.; Wang, H.H.; Kini, A.M.; Whangbo, M.H. Organic Superconductors (Including Fullerenes). In *Synthesis, Structure, Properties and Theory*; Prentice Hall: Englewood Cliffs, NJ, USA, 1992.
3. Shimizu, Y.; Hiramatsu, T.; Maesato, M.; Otsuka, A.; Yamochi, H.; Ono, A.; Itoh, M.; Yoshida, M.; Takigawa, M.; Yoshida, Y.; et al. Pressure-Tuned Exchange Coupling of a Quantum Spin Liquid in the Molecular Triangular Lattice κ -(ET)₂Ag₂(CN)₃. *Phys. Rev. Lett.* **2016**, *117*, 107203. [[CrossRef](#)] [[PubMed](#)]
4. Hassan, N.; Cunningham, S.; Mourigal, M.; Zhilyaeva, E.I.; Torunova, S.A.; Lyubovskaya, R.N.; Schlueter, J.A.; Drichko, N. Evidence for a quantum dipole liquid state in an organic quasi-two-dimensional material. *Science* **2018**, *360*, 1101–1104. [[CrossRef](#)] [[PubMed](#)]
5. Lyubovskaya, R.; Zhilyaeva, E.; Shilov, G.; Audouard, A.; Vignolles, D.; Canadell, E.; Pesotskii, S.; Lyubovskii, R. Dual-Layered Quasi-Two-Dimensional Organic Conductors with Presumable Incoherent Electron Transport. *Eur. J. Inorg. Chem.* **2014**, *2014*, 3820–3836. [[CrossRef](#)]

6. Saito, G.; Yoshida, Y. Development of Conductive Organic Molecular Assemblies: Organic Metals, Superconductors, and Exotic Functional Materials. *Bull. Chem. Soc. Jpn.* **2007**, *80*, 1–137. [[CrossRef](#)]
7. Fourmigué, M.; Batail, P. Activation of Hydrogen- and Halogen-Bonding Interactions in Tetrathiafulvalene-Based Crystalline Molecular Conductors. *Chem. Rev.* **2004**, *104*, 5379–5418. [[CrossRef](#)] [[PubMed](#)]
8. Kobayashi, H.; Cui, H.; Kobayashi, A. Organic Metals and Superconductors Based on BETS (BETS = Bis(ethylenedithio)tetrathiafulvalene). *Chem. Rev.* **2004**, *104*, 5265–5288. [[CrossRef](#)] [[PubMed](#)]
9. Sessoli, R.; Gatteschi, D.; Caneschi, A.; Novak, M.A. Magnetic bistability in a metal-ion cluster. *Nature* **1993**, *365*, 141–143. [[CrossRef](#)]
10. Zabala-Lekuona, A.; Seco, J.M.; Colacio, E. Single-Molecule Magnets: From Mn12-ac to dysprosium metallocenes, a travel in time. *Coord. Chem. Rev.* **2021**, *441*, 213984. [[CrossRef](#)]
11. Shen, Y.; Ito, H.; Zhang, H.; Yamochi, H.; Katagiri, S.; Yoshina, S.K.; Otsuka, A.; Ishikawa, M.; Cosquer, G.; Uchida, K.; et al. Simultaneous manifestation of metallic conductivity and single-molecule magnetism in a layered molecule-based compound. *Chem. Sci.* **2020**, *11*, 11154–11161. [[CrossRef](#)] [[PubMed](#)]
12. Kushch, N.D.; Buravov, L.I.; Kushch, P.P.; Shilov, G.V.; Yamochi, H.; Ishikawa, M.; Otsuka, A.; Shakin, A.A.; Maximova, O.V.; Volkova, O.S.; et al. Multifunctional Compound Combining Conductivity and Single-Molecule Magnetism in the Same Temperature Range. *Inorg. Chem.* **2018**, *57*, 2386–2389. [[CrossRef](#)] [[PubMed](#)]
13. Tamura, M.; Matsuzaki, F.; Nishio, Y.; Kajita, K.; Kitazawa, T.; Mori, H.; Tanaka, S. Novel BEDT-TTF salts containing rare earth ions, (ET)₄Ln(NCS)₆·CH₂Cl₂. *Synth. Met.* **1999**, *102*, 1716–1717. [[CrossRef](#)]
14. Kushch, N.; Kazheva, O.; Gritsenko, V.; Buravov, L.; Van, K.; Dyachenko, O. Novel packing type of ET radical cation layers in a new organic conductor (ET)₅[Dy(NCS)₆NO₃]·C₂H₅OH with a metal-complex lanthanide anion. *Synth. Met.* **2001**, *123*, 171–177. [[CrossRef](#)]
15. Shen, Y.; Cosquer, G.; Breedlove, B.K.; Yamashita, M. Hybrid Molecular Compound Exhibiting Slow Magnetic Relaxation and Electrical Conductivity. *Magnetochemistry* **2016**, *2*, 44. [[CrossRef](#)]
16. Imakubo, T.; Sawa, H.; Tajima, H.; Kato, R. Novel organic conductors containing lanthanide element in counter anion. *Synth. Met.* **1997**, *86*, 2047–2048. [[CrossRef](#)]
17. Kobayashi, H.; Kobayashi, A.; Sasaki, Y.; Saito, G.; Inokuchi, H. The crystal structures of (BEDT-TTF)ReO₄(THF)_{0.5} and (BEDT-TTF)IO₄(THF)_{0.5}. *Chem. Lett.* **1984**, *183*, 183–186. [[CrossRef](#)]
18. Guionneau, P.; Kepert, C.; Bravic, G.; Chasseau, D.; Truter, M.; Kurmoo, M.; Day, P. Determining the charge distribution in BEDT-TTF salts. *Synth. Met.* **1997**, *86*, 1973–1974. [[CrossRef](#)]
19. Benelli, C.; Gatteschi, D. Magnetism of Lanthanides in Molecular Materials with Transition-Metal Ions and Organic Radicals. *Chem. Rev.* **2002**, *102*, 2369–2388. [[CrossRef](#)] [[PubMed](#)]
20. Konarev, D.V.; Khasanov, S.S.; Batov, M.S.; Martynov, A.G.; Nefedova, I.V.; Gorbunova, Y.G.; Otsuka, A.; Yamochi, H.; Kitagawa, H.; Lyubovskaya, R.N. Effect of One- and Two-Electron Reduction of Terbium(III) Double-Decker Phthalocyanine on Single-Ion Magnet Behavior and NIR Absorption. *Inorg. Chem.* **2019**, *58*, 5058–5068. [[CrossRef](#)] [[PubMed](#)]
21. Konarev, D.V.; Zorina, L.V.; Batov, M.S.; Khasanov, S.S.; Otsuka, A.; Yamochi, H.; Kitagawa, H.; Lyubovskaya, R.N. Optical and magnetic properties of *trans*-indigo^{•−} radical anions. Magnetic coupling between *trans*-indigo^{•−} (*S* = 1/2) mediated by intermolecular hydrogen N–H···O=C bonds. *New J. Chem.* **2019**, *43*, 7350–7354. [[CrossRef](#)]
22. Shintoyo, S.; Murakami, K.; Fujinami, T.; Matsumoto, N.; Mochida, N.; Ishida, T.; Sunatsuki, Y.; Watanabe, M.; Tsuchimoto, M.; Mrozinski, J.; et al. Crystal Field Splitting of the Ground State of Terbium(III) and Dysprosium(III) Complexes with a Triimidazolyl Tripod Ligand and an Acetate Determined by Magnetic Analysis and Luminescence. *Inorg. Chem.* **2014**, *53*, 10359–10369. [[CrossRef](#)] [[PubMed](#)]
23. Goodwin, C.A.P. Blocking like it's hot: A synthetic chemists' path to high-temperature lanthanide single molecule magnets. *Dalton Trans.* **2020**, *49*, 14320–14337. [[CrossRef](#)] [[PubMed](#)]
24. Bonner, J.C.; Fisher, M.E. Linear Magnetic Chains with Anisotropic Coupling. *Phys. Rev.* **1964**, *135*, A640–A658. [[CrossRef](#)]
25. Estes, W.E.; Gavel, D.P.; Hatfield, W.E.; Hodgson, D.J. Magnetic and structural characterization of dibromo- and dichloro-bis(thiazole)copper(II). *Inorg. Chem.* **1978**, *17*, 1415–1421. [[CrossRef](#)]
26. Agilent. *CrysAlis PRO*, Version 171.35.19; Agilent Technologies UK Ltd.: Oxfordshire, UK, 2011.
27. Sheldrick, G.M. Crystal structure refinement with *SHELXL*. *Acta Crystallogr. Sect. C Struct. Chem.* **2015**, *C71*, 3–8. [[CrossRef](#)] [[PubMed](#)]